Distributed Vision Sensing of Small Uncrewed Aircraft Systems in Urban Traffic Corridors

Chester V. Dolph[1], Dasarath Katragadda [2] Todd Ferrante[3],
NASA Langley Research Center, Hampton, Virginia 23681

Thomas Lombaerts[4], Corey Ippolito[5], Vahram Stepanyan[6], Evan Kawamura[7],
NASA Ames Research Center, Moffett Field, CA, 94035

Federica Vitiello [8], Flavia Causa [9], Roberto Opromolla [10], Giancarmine Fasano [11]
University of Naples Federico II, Naples, Italy

The NASA Advanced Air Mobility mission will enable widespread low altitude passenger travel, cargo delivery, and a variety of public services through the development of Uncrewed Aerial Systems (UAS) operations. Ensuring safe, autonomous operations in densely populated environments requires careful consideration towards hazards including other aircraft, infrastructure, and evolving weather. Small Uncrewed Aerial Systems (SUAS) present a unique hazard to UAS operations as they share airspace and may be readily operated in a non-cooperative fashion. This work investigates distributed sensing of SUAS traversing an air traffic corridor in an urban setting. This work develops a distributed vision detect and track strategy at NASA Langley Research Center. Three nodes, each with at least one global shutter camera, are distributed around a traffic corridor to surveil flight operations for two SUAS performing low altitude flight operations. Each node is equipped with a GPS and cellular modem to enable timestamping and remote control of acquisition. Node one faces a traffic roundabout with buildings in the background and achieves 99% surveillance coverage for two SUAS against building and tree backgrounds at ranges 50 to 130m. The second node points down Langley Boulevard with trees and buildings in the background and achieves 99% coverage at separation distances between 70 and 180m. The analysis for the second node is limited to ranges below 180m due to low contrast against dark, tree backgrounds. Finally, the third node points down Langley Boulevard from another perspective and achieves 99% coverage at ranges 60m to 200m against mostly building with a few sections of trees in the background.

I. Introduction

NASA's Advanced Air Mobility (AAM) mission will transform airspace through the movement of people and cargo in UAS in urban, rural, and suburban environments [1]. Applications for autonomous AAM aircraft include emergency response after natural disasters as search and rescue vehicles, transport medical supplies and serve as an ambulance, move cargo efficiently, carry people between destinations to reduce travel time, and improve commutes using vertiports [2]. AAM's High Density Vertiport (HDV) flight campaign [3] [4] advanced autonomous flight

[1] Aerospace Engineer, Aeronautics Systems Engineering Branch, AIAA Senior Member.
[2] Computer Vision Intern, Aeronautics Systems Engineering Branch, AIAA Student Member.
[3] Robotics Engineer, Analytical Mechanics Associates, Inc. NASA Langley Research Center.
[4] Aerospace Research Engineer, KBR Wyle Services, Intelligent Systems Division, AIAA Associate Fellow
[5] Aerospace Scientist, Intelligent Systems Division. NASA Ames. AIAA Senior Member.
[6] ESOF40-Technical Advisor, KBR Wyle Services, Intelligent Systems Division
[7] Aerospace Scientist, Intelligent Systems Division. NASA Ames. AIAA Senior Member.
[8] Postdoctoral Scholar, Department of Industrial Engineering, University of Naples "Federico II".
[9] Postdoctoral Scholar, Department of Industrial Engineering, University of Naples "Federico II".
[10] Assistant Professor, Department of Industrial Engineering, University of Naples "Federico II".
[11] Associate Professor, Department of Industrial Engineering, University of Naples "Federico II".

operations through the development of complex SUAS missions with remote control. NASA's Transformational Tools and Technology (TTT) project supports the AAM mission through the Revolutionary Aviation Mobility subproject [5] in these areas:

1. Developing and field-testing Remote Operations for Autonomous Missions (ROAM), a NASA developed traffic management system, for Multi-Vehicle (*m*:*N*) Operations where *m* operators, ground control operators, control *N* operations [6].
2. Conducting Human-in-the-Loop (HITL) experiments to develop safe human-autonomy traffic management systems [7]
3. Developing Intelligent Contingency Management (ICM) strategies for safely handling unforeseen off-nominal aircraft operations [8]
4. Developing electric Vertical Take Off and Land (eVTOL) SUAS [9]
5. Developing distributed sensing architectures to surveil AAM airspace [10] [11] [12].

Sensing strategies for AAM aim to enable safe, widespread autonomous operations through surveillance using distributed sensors. Recent TTT and partner contributions in distributed sensing areas include: sensor fusion strategies [13], surveillance strategies [14] [15] [16] [17] [18] [19] [20], and simulation of AAM/UAM environment towards developing a Concept of Operations [21] [22].

This work develops a distributed sensing vision architecture in the context of air traffic corridors. This manuscript is organized as follows: contributions, related works, sensing techniques, experimental methodology, results, discussion, and conclusion.

II. Related Works

Various approaches for SUAS detection exist in the literature using varying modalities, sensors, and experimental environments. The current work has explored the usage of standard computer vision algorithms, neural networks, radar-based detections, and audio detection. Vision strategies tend to be highly accurate at close and distant ranges, however they are limited in adverse visibility conditions (night, rain, fog, etc.). Thermal vision has been used to bolster vision performance in adverse conditions [23]. Radar-based detection is more robust in degraded visual conditions; however, the angular resolution of radar-based methods is substantially lower than vision systems [24]. Audio detection has limitations regarding range and generalizability due to background noise sources and suffers from signal attenuation as distance increases [25].

The approaches to tracking vehicles are largely based on the Kalman filter with an association strategy. While algorithms may differ, the overall approach is to initialize tracks, use a Kalman Filter to predict the future location of each track, and verify in the next frames whether there is a detection at the predicted location [26]. Convolutional neural networks and deep siamese networks may be used for detection, however work regarding object tracking with neural networks in the UAM field is not fully explored [27].

Current datasets used for SUAS detection are limited. While many datasets have been collected and compiled, most are limited in at least one aspect. These datasets either contain low resolution images, limited annotating, or non-existent ground truths to validate against, or do not cover scenarios expected in the urban usage of SUAS vehicles found in the UAM vision [28]. One common issue with publicly available datasets is that the recordings are compilations of videos from the internet, and not standalone aviation datasets collected in controlled environments [27]. This is a major limitation for the development of SUAS detection and tracking methodologies, as without robust, labeled, high fidelity datasets, any proposed solutions are unable to be verified. This paper utilizes a dataset that aims to advance SUAS surveillance work within the UAM context.

III. Contributions

This work advances autonomous SUAS and AAM through the development of distributed vision strategies. The key contribution of this research is field-testing distributed sensing visual surveillance strategies in an urban environment. The architecture of the detection and tracking strategy is an extension of an airborne version developed in [14] and adapted to the urban environment through the augmentation of pipeline by adding a new subtraction methodology.

IV. Vision Sensing Techniques and Evaluation Metrics

This section details the visual sensing architecture used to detect and track SUAS vehicles. This detect and track processing pipeline, as shown in Figure 1, is built in Python and C++. The pipeline is fed a frame from one of the sensing nodes and detects any SUAS vehicles using various combinations of a differential, morphological, and background subtraction detector. The detections are then fed into the tracker, which utilizes a Kalman filter to model the same object's path across sequential frames. The detections, tracks, and annotated images are then outputted for analysis. The detector is written in python to facilitate simple testing and implementation of novel detection strategies, and the tracker is written in C++ to optimize runtime. Runtime of the python detector is not impacted significantly as OpenCV's backend is written in C++ [29]. The tracker is built into a python library using PyBind11 for simple integration.

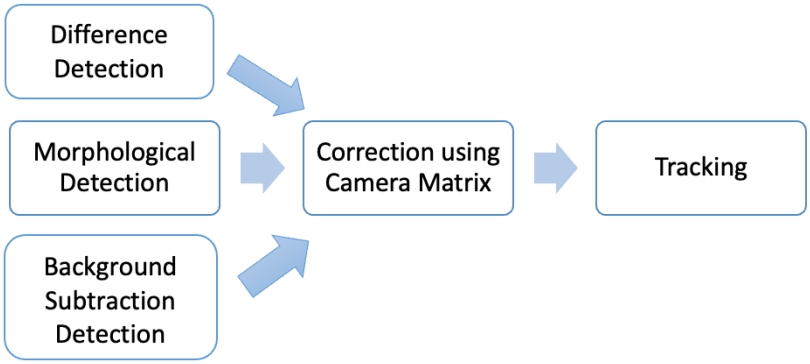

Figure 1: Detect and Track Pipeline.

A. Detection Methods

Three unique detection methodologies are evaluated: a Features from Accelerated Segment Test (FAST) [30] based image differencing detector, a morphological detector, and an image differencing detector. The morphological and contour differencing were developed and detailed in [14] for airborne detection of general aviation aircraft, fixed-wing SUAS, and multirotor SUAS from both multirotor and fixed-wing SUAS. A summary of these detectors is presented below.

The FAST image differencing technique includes converting to grayscale and an initial gaussian blur step to suppress detections from high texture backgrounds. This is followed by FAST keypoint [31] detection for both current and previous frame as shown in Error! Reference source not found.. The Lucas Kanade Optical Flow algorithm [32] projects the FAST features from the previous frame into current frame in order to associate current and previous features to compute homography. The resulting homography matrix is used to transform the previous frame into the current frame, thus minimizing interframe change in the case of moving a camera. The absolute difference between the previous transform frame and the current frame is computed. A feature detection threshold, which is varied in the analysis of this work, is used to extract moving objects using the FAST feature threshold. The FAST feature threshold is increased until the number of detections is below the maximum allowed feature detection threshold. Too many detections may saturate a tracking system with unnecessary detections; however, detecting SUAS against cluttered tree background with low contrast may require a higher detection threshold. This tradeoff must be balanced to optimize tracking results.

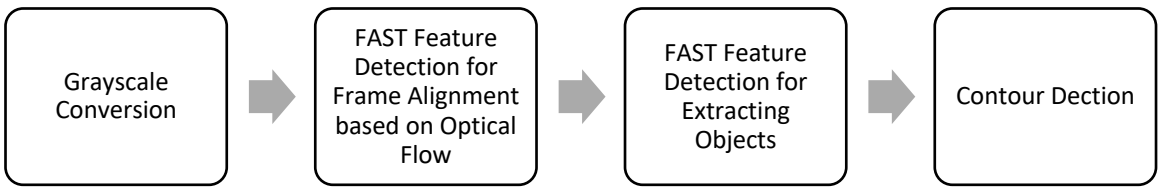

Figure 2: Differential Detection Process.

The morphological filtering technique uses a standard close-minus-open filter to extract SUAS after converting to grayscale. A 5 by 5 cross hair kernel is used in the filtering and is based on work in [33] developed for detecting general aviation aircraft at great ranges. Once the image is filtered, the same FAST feature detection methodology from the difference detector is used.

A second image differencing technique, referred to as subtraction in this work, was implemented to increase coverage with the dark, mostly black, SUAS against low contrast black tree backgrounds. This methodology, demonstrated in Figure 3, is based off [34] where low contrast SUAS were detected from static cameras. The image is first converted to grayscale, and then a MOG2 background subtraction algorithm is used to remove most non-moving artifacts. After the background is subtracted, the image is converted to binarized with a thresholding step, and then the image is eroded to remove any small artifacts. Afterwards, the image is dilated to eliminate multiple detections on the same object. Finally, contour detection and centroiding is run on the image to determine the location of each object.

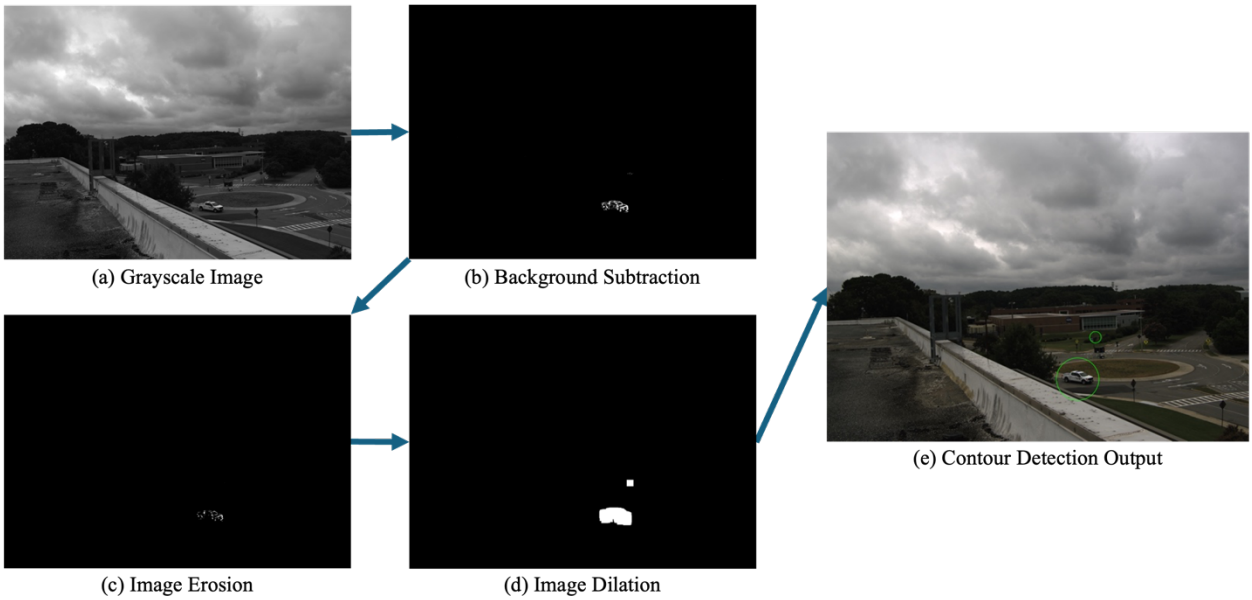

Figure 3:Background Subtraction Detection Process.

B. Tracking Algorithm

The tracking method shown in Figure 4 was initially developed in [35] and [36]. The detector input to the tracker is first clustered using the Density-Based Spatial Clustering of Applications with Noise (DBSCAN) algorithm [37] to minimize duplicate tracks. Unlike the detection process, tracking occurs in a corrected coordinate space to minimize the effect of radial and tangential distortion. Camera calibration is performed using the Bouguet camera calibration toolbox [38]. The tracker is structured in three main tracking blocks: the One-Plot tracker, the Tentative tracker, and the Firm tracker. The first block, the One-Plot tracker, generates initial track estimates starting from visual measurements. Once generated, a One-Plot track can become Tentative if its association with new measurements is verified. The Tentative tracker block is thus an intermediate phase which will yield a firm track upon further association verification. The Firm tracker is the last stage of the tracking chain and represents the highest reliability level. During firm tracking, linear Kalman filters are used to estimate the relative location of targets in terms of their azimuth and elevation angles with respect to the camera. At this stage, tracks are predicted using a Nearly Constant Velocity (NCV) dynamic model and corrected using Kalman filtering. Firm tracks are maintained for a pre-defined time after which, if no measurement has associated, tracks are deleted. At all stages, association is verified by comparing the Euclidean distance between the measurement and the track prediction with a pre-defined threshold. At One-Plot and Tentative levels, which do not foresee any track prediction, the Euclidean distance is measured using previous and current measurements.

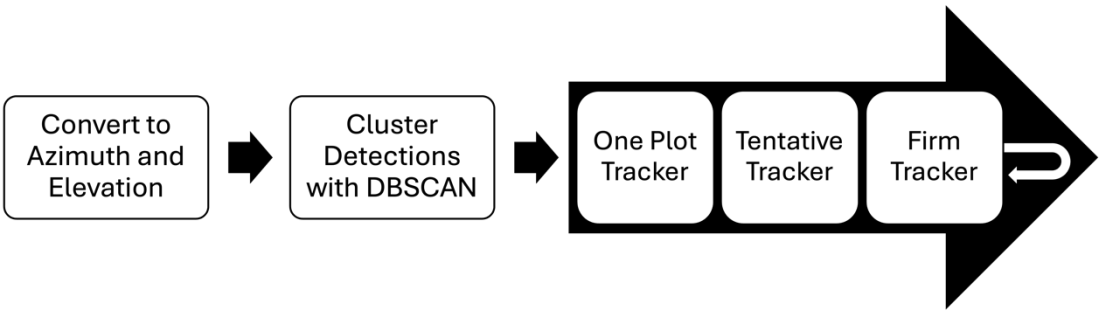

Figure 4: Tracker Process

C. Vision Algorithm Tuning and Performance Metric

A primary objective of this work was to evaluate how varying vision algorithms perform at extracting SUAS in urban environments. Maximum detection keypoint thresholds of 15, 30, 45, 90, and 180 are evaluated to understand the impact of SUAS coverage. Outputs from the tracker are computed on each individual detection output, the combined detection outputs, and the combined morphological and differential detector outputs.

The tracking algorithms were evaluated using tracker coverage when the SUAS is present. Tracker coverage is calculated by dividing the number of tracker hits divided by the number of frames where the SUAS is present. A tracker hit occurs when the L2 norm between the tracker output and the ground truth (extracted from GPS log from each SUAS) is below the association threshold. The GPS coordinates for the SUAS are transformed into a local North East Down reference frame using the **QU**aternion **EST**imator (QUEST) algorithm [39] as detailed in the following experimental methodology section.

V. Experimental Methodology

This section provides a description of the SUAS experiment including aircraft performance characteristics. The urban flight simulation used in this study was a portion of a flight test campaign within NASA Langley Research Center's campus. Data acquisition occurred on the 7th of September 2024 on a cloudy, overcast day. The collected dataset from this flight test consists of approximately 30000 frames spread across three sensing nodes. Of these frames, approximately 6000 frames contain SUAS within the FOV of a ground node. As discussed in the experimental methods section, the sky was cloudy, yielding lower contrast between the vehicles and clear sky.

A. Test Procedures

The flight test for this experiment took place along the main street, Langley Boulevard, within NASA Langley's campus as shown in Figure 5 with altitude and speed in Table 1. As this campaign aimed to simulate SUAS flight through an urban environment, the test took place in a location containing buildings, roads, traffic signs, trees, and many other objects creating partial occlusion and low contrast scenarios. The sky was cloudy, creating a gray background which reduced contrast between the vehicles and the sky.

The aircraft used in this flight campaign consisted of one Alta-8 and one Alta-X SUAS. Both vehicles contained GPS units to provide ground truth data to validate the detect and track pipeline results. The flightpath of the vehicles, as seen in Figure 5, consisted of a single loop around the northwest/southeast segment of Langley Bvld. The vehicles

took off, traveled northwest until reaching the turnaround coordinates, traveled southeast until reaching the roundabout, and then returned to the route's starting location.

Figure 5: Flight Path of Alta 8 and Alta X Vehicles.

Table 1: Aircraft Altitude and Speed.

SUAS	Altitude (ft)	Average Speed (kilometers per hour)
Alta X	20	7.1
Alta 8	25	8.4

B. Sensor Nodes

The nodes are configured with the sensors as shown in Table 2 with companion computers and GPS as described in detail in Table 3. All NASA node cameras have a Sony IMX253 or Sony IMX304 sensors as well as an Echodyne Echoflight radar. C1 is shown in Figure 6 and includes 3 cameras and 1 radar mounted to a tripod on top of NASA Langley's Building 1232 facing the Langley Boulevard roundabout. The three cameras have a 1 degree overlap in Field Of View (FOV) yielding a combined horizontal FOV of 139.9 with a vertical FOV of 36.1. C2, the single camera Xavier node shown in Figure 7, is mounted on a tripod on 1232 facing the takeoff area pointing in the Northwestern direction. C3, the single camera Nuc node on NASA Langley Building 1268, is shown in Figure 8, and faces the southeastern direction on Langley Boulevard towards building 1232. C4 is shown in Figure 9 with integrated batteries to supply power, however, is not included in the analysis for this work due requiring a separate data labeling procedure. The analysis presented in this report is constrained to 1 camera per node without radar utilization.

Table 2: Node Sensor Configuration.

Node	Camera Model	Camera Resolution (pixels)	Horizontal and vertical Lens FOV (degrees)
C1	BFS-U3-123S6C-C	4096 x 3000	47.3 x 36.1
C2	BFS-U3-123S6C-C	4096 x 3000	62.5 x 47.8
C3	BFS-U3-122S6C-C	4096 × 3000	62.5 x 47.8
C4	BFS-U3-123S6C-C	4096 x 3000	62.5 x 47.8

Table 3: Node GPS and Computer Configuration.

Node	Differential GPS	Computer	Cellular Modem
C1	Sparkfun GPS-RTK-SMA ZED-F9P (Ublox)	3 Xaviers with Contech Rogue breakout Board	RUTX11
C2	Sparkfun GPS-RTK-SMA ZED-F9P (Ublox)	Xaviers with Contech Rogue breakout Board	RUTX11
C3	Sparkfun GPS-RTK-SMA ZED-F9P (Ublox)	NUC 11 Performance Mini Desktop Computer,	RUTX11
C4	BFS- Sparkfun GPS-RTK-SMA ZED-F9P (Ublox)	Xaviers with Contech Rogue breakout Board	RUTX11

Figure 6: C1 on 1232 facing traffic Langley Boulevard circle.

Figure 7: C2 on 1232 building facing down Langley Boulevard towards Building 1268.

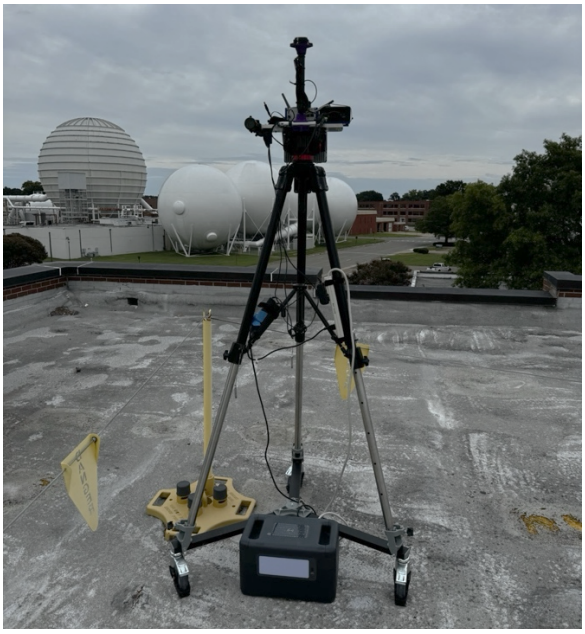

Figure 8: C3 on 1268 rooftop facing down Langley Boulevard towards Building 1232.

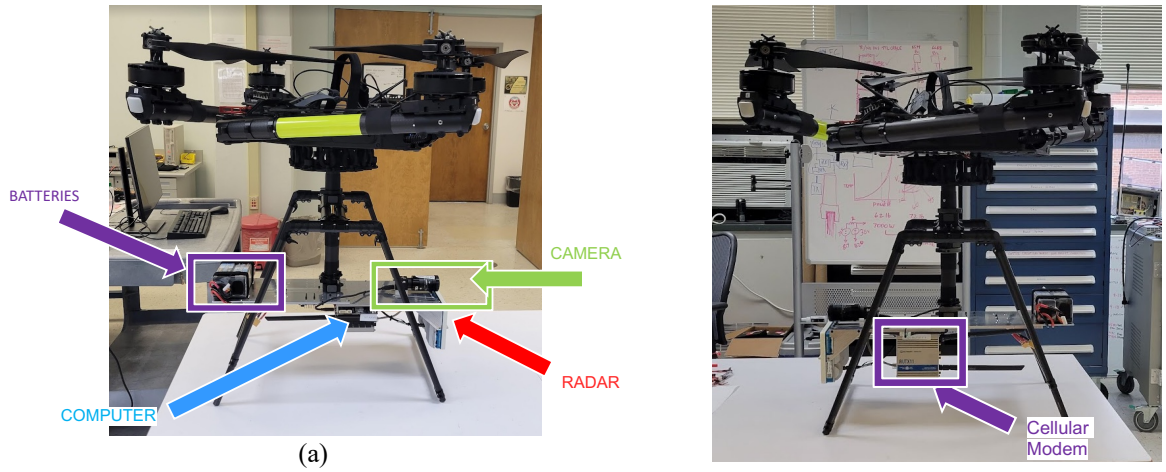

(a) (b)

Figure 9: Onboard Payload as seen from port (a) and starboard (b) sides with research payload annotated.

Figure 10: Node Locations and Orientations.

C. Description of Target Aircraft

The aircraft are shown in proximity to takeoff in Figure 11. The technical specifications of the HDV Alta 8 SUAS are detailed in Table 4.

Figure 11: Alta 8, smaller SUAS on left, and taller and larger Alta X on right. Also included are flight test team (left to right: Dave North, Brian Duvall, Todd Ferrante, Chester Dolph, Dasarath Katragadda, Elanor Finlayson, Jacob Schaefer, Imran Khasawneh, Jody Miller, Skyler Hudson, Brayden Chamberlain, Officer Alfred (Al) Knight, Officer Nicollo (Nico) Petrosino).

Table 4:Alta 8 specifications.

SUAS Type	Multi-Rotor, 8 Motor (Brushless)
Diagonal Length	52 in (1.3 m) *Does not include Props
Maximum Weight	40 lbs. (18.14 kg)
Empty Weight	13.6 lbs. (6.2 kg)
Propulsion Battery	6-cell Li-Poly (Nominal 22.2V)
Speed	0 –30 kts (0-15.4m/s)
Max Flight Time	34 mins
Operating Frequency	2.4 GHz RCTX C2 (~2 Miles) 900 MHz C2 & Flight Data (~3 Miles) 700MHz/1700MHz C2 & Flight Data
Command and Control	RC TX & Laptop

D. Description of Aircraft with Payload

The technical specifications of the HDV SUAS are detailed in Table 5.

Table 5: Alta X specifications.

SUAS Type	Multi-Rotor, 4 Motor (Brushless)
Diagonal Length	89.5 in (2.27 m)
Maximum Weight	76.9 lbs. (34.9 kg)
Empty Weight	22.9 lbs. (10.4 kg)
Propulsion Battery	12-cell Li-Ion (Nominal 44.4V)
Speed	0 – 38.8 kts (0-20.0m/s)
Max Flight Time	50 mins
Operating Frequency	2.4 GHz RC TX C2 (~2 Miles) FRX 900 MHz Telemetry radio (~1 Mile)
Command and Control	RC TX & Laptop

E. Data Labeling Procedure

The attitude of the camera in the North East Down (NED) reference frame, shown in Figure 12, is computed using QUEST with manual labeling of the Alta 8 in 20 frames and GPS logs of SUAS and sensor nodes. Frame selection captured a variety of positions within the Alta 8 path, however, variation in elevation angles were limited as the SUAS did not generally translate in the vertical direction in image space. After selecting frames, the centroid pixels were manually identified. Finally, the attitude is computed with the QUEST algorithm using the time synchronized pixel coordinate labels, the GPS coordinates of the Alta 8, and the GPS coordinates of the sensor nodes.

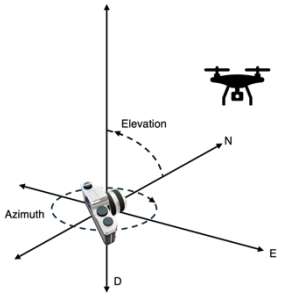

Figure 12: Sensor Reference Frame.

VI. Results

This section discusses the results of the track outputs from the processing pipeline. It covers the performance of the tracker and detectors, the track deviation from the ground truths, and the percentage coverage of the SUAS.

A. Tracker Output on Ground Truth NED

The output of each tracker was visualized on angular plots such as the one shown in Figure 13 to confirm vision trackers were achieving accurate azimuth and elevation results when superimposed upon the ground truth. Initial parameters for ground truth hit threshold for the L2 norm between the ground truth and the SUAS were 1 and 2 degrees respectively. However, the results show a vertical offset as highlighted in the red box in Figure 13. Likely reasons for this offset include limited elevation angles used when labeling the data in the Alta 8 in vision space or that the Alta X includes an increase in altitude for approximately 1 minute between ~320 and 380 seconds. Another possible explanation is that altitude computed from GPS is typically accurate to 2-3m horizontally and 10 m vertically; thus, performing QUEST on Alta 8 and not Alta X may enable accurate association with the Alta 8 but not Alta X. Operating below building heights results in multipathing of GPS signal along with variations in satellite numbers due to occlusions from structures. Strategies to mitigate this include using a SUAS to cover the sensor FOV at greater ranges - when possible - to enable more accurate transformations through coverage or using additional known references within the frame (i.e. GPS coordinates of building, stop sign, etc.). To verify alignment between QUEST transformations and tracker outputs, a manual track verification procedure was used on a sample of the dataset, along with a mitigation strategy that increased the degree threshold for a hit to 4 degrees.

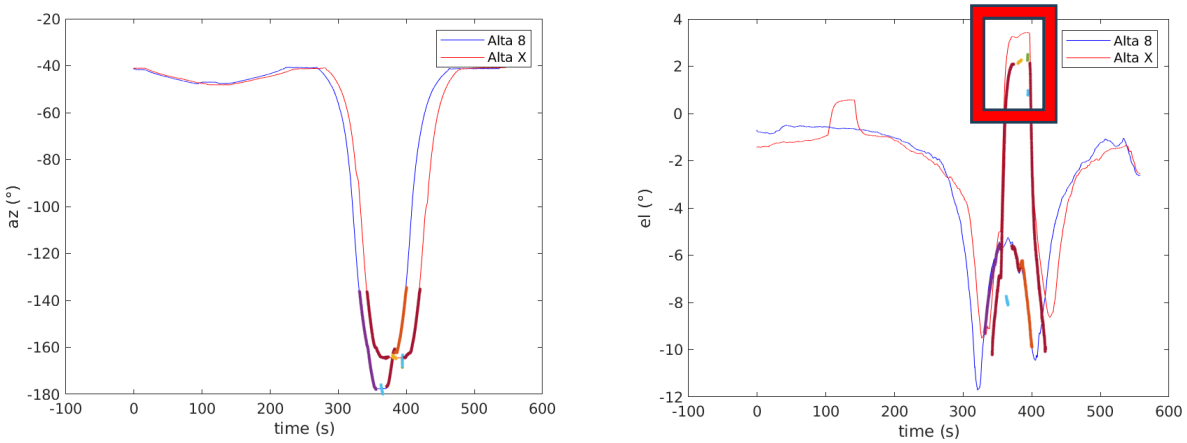

(a) (b)

Figure 13: Background Subtraction Tracker Output on Angular Plots for C1 for azimuth elevation angles (a) and elevation angles (b) in degrees with offset highlighted in red box. The bolded lines represent the output from the Background Tracker.

B. Tracker Coverage

Tracker coverage plots are shown in Figure 14 through Figure 18, where the horizontal axis corresponds to tracker coverage of the Alta 8 and the vertical axis Alta X respectively. In each figure, "D" corresponds to the contour image difference detector, "M" corresponds to the morphological detector, "S" corresponds to the background subtraction difference detector, "DMS" is all three detectors combined as inputs into the Kalman filter, and "DM" is the difference and morphological detectors combined. Trends across cameras generally show that higher maximum feature thresholds improve tracker coverage for both SUAS and combining all three detectors will yield 99% tracker coverage in each scenario.

C1 faces a mixture of trees and buildings in the background with the SUAS closer in distance relative to C2 and C3. This allows for the use of lower detection thresholds, with a threshold of 15 achieving over 95% coverage for both SUAS. C1 also captures two additional transition cases not captured in C2 and C3: the case where the Alta X increases its altitude, and where the Alta 8 is momentarily stationary during the transition from departure to arrival on Langley Boulevard. Neither of these transition cases present significant challenges to the detect-track methodology, as high tracking performance is achieved across both. Generally, the morphological detection methodology performed poorly across thresholds. This may be attributed to the high texture background generating many detections unrelated to SUAS as it is essentially a corner detector and there are many corners in the imagery. However, the detector which achieved the highest tracking performance at a threshold of 15 on C1 includes the morphological detector input.

C2's FOV captures the greatest distance down Langley Boulevard, with dense foliage presenting challenges for detecting black SUAS against low contrast tree-backgrounds. SUAS detections for C2 node were low for both SUAS at great distances on textured backgrounds due to the low-contrast and relatively small vehicle size in pixel space. However, in the scenarios where C2 did not track the SUAS due to range, the C3 node was able to compensate and track the vehicles successfully. In C2, several objects including cars and people generated tracks within 1 degree of the SUAS at distances beyond 180m. Thus, discerning between non-SUAS and SUAS became difficult due to the proximity of objects to the SUAS and the inaccuracy of the transform from QUEST. Therefore, frames where SUAS were out of the detection range of C2 were excluded from this analysis. In C2, tracker performance for the Alta X is generally higher at lower detection thresholds than the Alta 8 for both SUAS arrivals, likely due to the white aperture of the radar generating a higher contrast relative to the radar-less Alta 8.

C3 captures buildings, wind tunnels spheres, and has a greater visual range relative to C1 without as many trees as C2 although trees are present in the background at greater separation distances between C3 and SUAS. Inspection of the annotated frames with tracking output show that performance suffers the greatest at range against low contrast backgrounds against trees and that increasing the detection feature threshold improves performance.

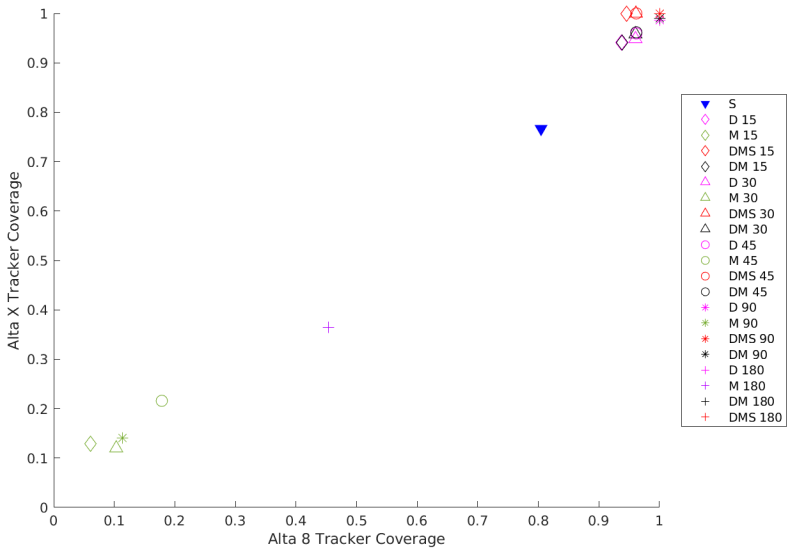

Figure 14: C1, traffic circle with a few buildings and trees.

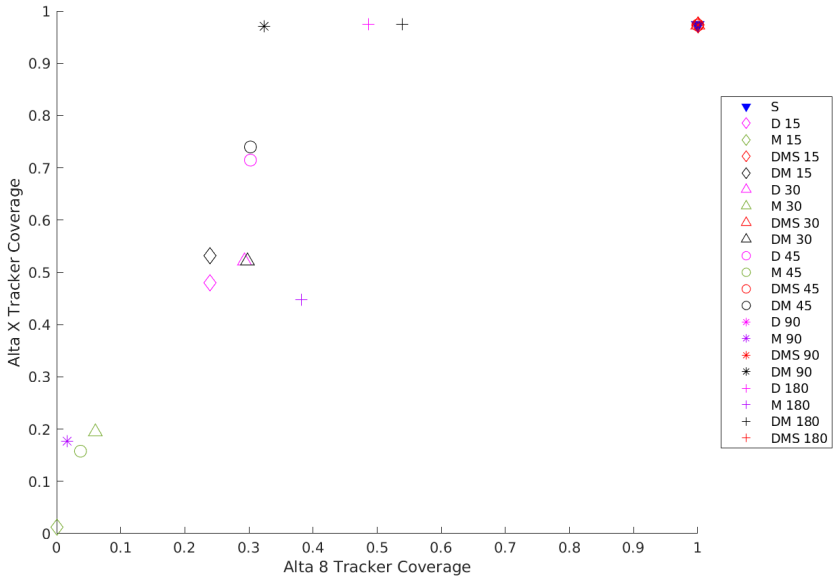

Figure 15: C2 Departure, SUAS on low contrast background for long approach.

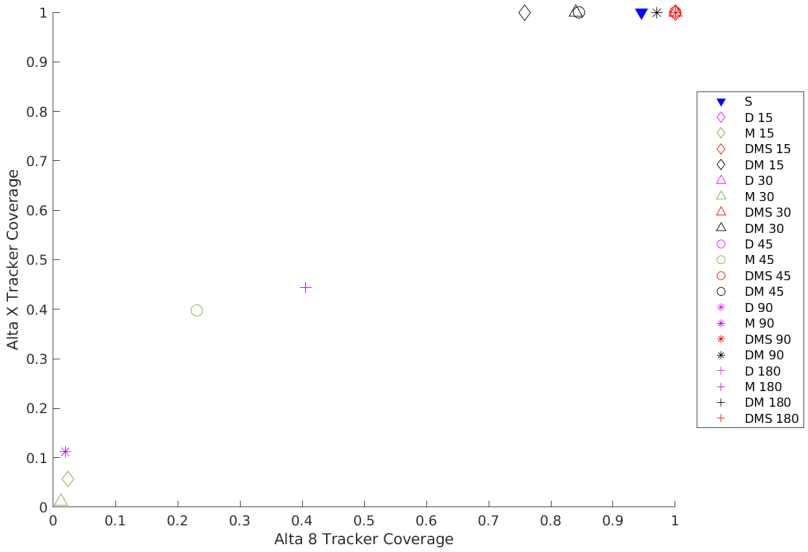

Figure 16: C2 Arrival, SUAS on low contrast background for departure.

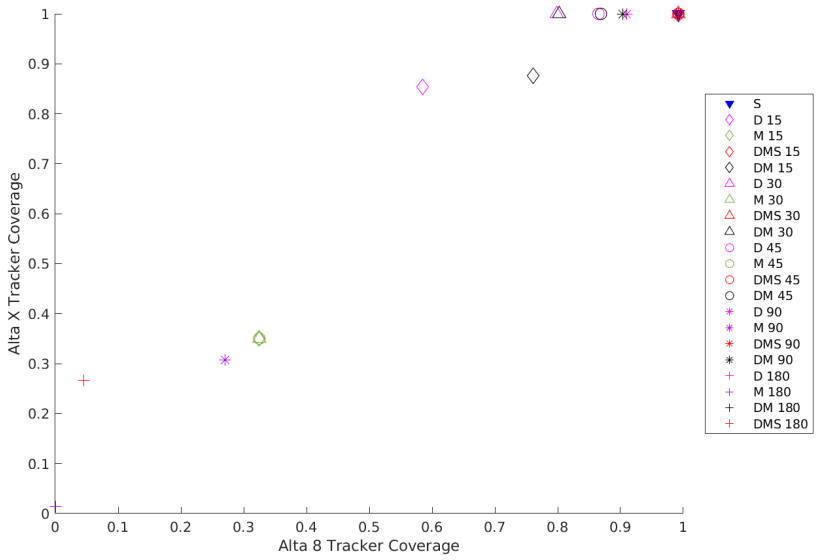

Figure 17: C3 Departure, SUAS on wind tunnel spheres and buildings.

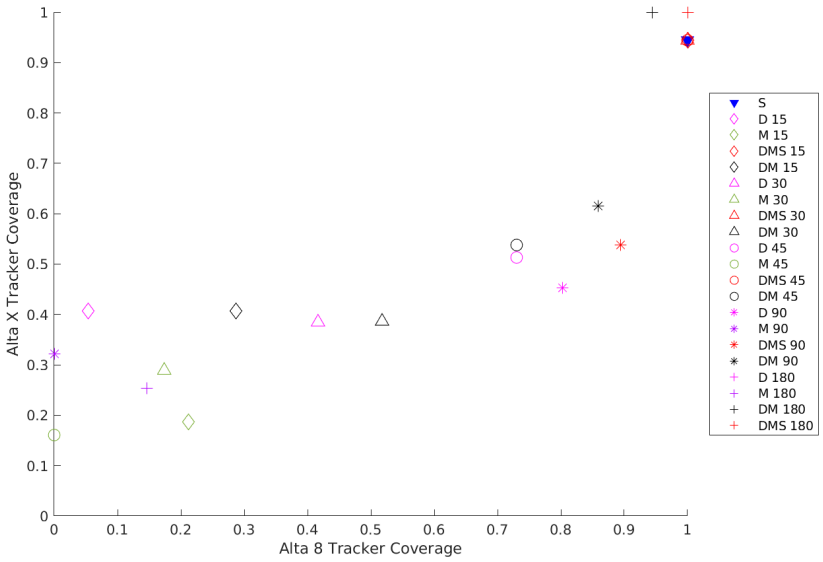

Figure 18: C3 Arrival, SUAS on wind tunnel spheres and buildings.

C. Runtime Performance

The pipeline was run on a local server containing an Intel Xeon Gold 6230 CPU, two Nvidia RTX A4000 GPUs, 512 GB of RAM, 2 TB of NVME SSD storage for saving results, and 64 terabytes of SSD for dataset storage. The runtime performance of the detection pipeline varied depending on image content. As seen in Table 6, the differential and morphological detector processed a single frame in approximately two seconds. Meanwhile, the background-subtraction based detector executed under a tenth of a second. This disparity is primarily due to the multiple instances of FAST Feature Detection utilized in both the differential and morphological detectors. The background subtractor

utilizes whole-image operations exclusively without the contour detection step for the morphological and difference detectors, which allows for a significantly faster runtime. The tracker executes over a tenth of a second for a single frame. Future enhancement will reduce runtime by limiting the amount of track information stored in system memory.

Table 6: Computation Performance of Varying Trackers.

Differential Detector	~1.80 seconds / frame
Morphological Detector	~2.20 seconds / frame
Background Subtraction Detector	~0.08 seconds / frame
Tracker	~0.15 seconds / frame

VII. Discussion

The highest detection threshold when combined with the subtraction technique achieved 99% or more tracking coverage of both SUAS within the selected frames for this work. Below the horizon and against textured backgrounds is of the most difficult tasks for small object detection. Admittedly, this analysis does not assess trackers for precision-recall analysis where unnecessary tracks at higher feature detection thresholds are quantified; however, assessing additional tracks proved to be time-consuming for this preliminary work given the number of moving objects within this dataset (cars, people, birds, etc.) and the lack of a highly accurate transform between the SUAS and the sensor reference frame. Furthermore, the morphological and difference detector pipeline were extensively evaluated in [14] from a moving multirotor SUAS for detecting General Aviation and fixed-wing SUAS. This evaluation included a precision-recall analysis to assess the number of unnecessary tracks. That work included an assessment of aircraft detections at ranges from 1 to nearly 4 kilometers across multiple days and backgrounds. A challenge for sensor-based detection strategies is generalizing a single technique to varying sensing conditions, backgrounds, and types of aircraft. In the present work, high tracking coverage was achieved at the highest thresholds while lower thresholds were successful to varying degrees.

Future work includes refining the QUEST transform strategy to yield higher data labeling performance with a Root Mean Square Error analysis between ground truth and tracker output. This will enable the visual detection and tracking pipeline to be optimized across multiple datasets, such as those presented in [4], and assessed using localization performance. Furthermore, the output of the tracks may be fed into a machine learning algorithm to provide object classification of SUAS, people, cars, and other objects of interest for AAM. Additional areas of future work include the development and analysis of the distributed sensing topology to ensure adequate coverage is provided for an UAM airspace.

VIII. Conclusion

This paper evaluates a distributed vision sensor system performance within the context of AAM traffic corridors using three remotely operated cameras deployed on rooftops in an urban-like environment. An analysis of optical based detection and tracking strategy is presented and demonstrates strong tracking performance of SUAS within the AAM context. Specific challenges include detecting black SUAS against trees and other low contrast backgrounds. Future objectives include scaling the process to additional datasets collected, integrating additional modalities, and applying machine learning to perform aerial object classification.

Acknowledgements

The authors would like to thank Imran Khasawneh, Dave North, Jacob Schaefer, Brian Duvall, Patrick Hill and Matt Coldsnow for their support in making this work possible. Additionally, the personnel shown in Figure 11 performed critical SUAS operational support roles including piloting, ground control operations, range safety, visual observer, and traffic control.

References

[1] W. Johnson and C. Silva, "NASA concept vehicles and the engineering of advanced air mobility aircraft," *The Aeronautical Journal,* vol. 126, pp. 55-91, 2022.

[2] T. Whiting, "NASA is Creating an Advanced Air Mobility Playbook," NASA, 2 Feb. 2023. [Online]. Available: https://www.nasa.gov/centers-and-facilities/armstrong/nasa-is-creating-an-advanced-air-mobility-playbook-2/. [Accessed 2 May 2024].

[3] L. Glaab, M. Johnson, R. McSwain, S. Geuther, Q. Dao and J. Homola, "The high density vertiplex advanced onboard automation overview.," in *IEEE/AIAA 41st Digital Avionics Systems Conference* , Portsmouth, 2022.

[4] C. Dolph, T. Lombaerts, C. Ippolito, V. Stepanyan, E. Kawamura, K. Kannan, G. Szatkowski, T. Ferante, C. Morris, F. Vitiello, F. Causa, R. Opromolla and G. Fasano, "Distributed Sensor Fusion of Ground and Air Nodes using Vision and Radar Modalities for Tracking Multirotor Small Uncrewed Air Systems and Birds," in *AIAA SciTech*, Orlando , 2024.

[5] V. Aubuchon, K. Hashemi, R. Shively and J. Wishart, "Multi-Vehicle (m:N) Operations in the NAS – NASA's Research Plans," in *AIAA AVIATION*, Chicago, 2022.

[6] B. Buck, E. Chancey, M. Politowicz, J. Unverricht and S. Geuther, "A Remote Vehicle Operations Center's Role in Collecting Human Factors Data," in *AIAA SciTech*, Orlando, 2023.

[7] J. Unverricht, B. Buck, B. Petty, E. Chancey, M. Politowicz and L. Glaab, "Vertiport Management from Simulation to Flight: Continued Human Factors Assessment of Vertiport Operations," in *AIAA SciTech*, Orlando, 2024.

[8] S. Ranganathan, H. Ilangovan, N. Campbell, M. Acheson and I. Gregory, "Off-Nominal Event Analysis in Autonomous Flights Based on Explainable Artificial Intelligence," in *AIAA SciTech*, Orlando 2024.

[9] S. Geuther, B. Simmons and K. Ackerman, "Overview of the Subscale RAVEN Flight Controls Testbed," in *Vertical Flight Society*, Montreal, 2024.

[10] C. Ippolito, E. Kawamura, G. Gorospe, W. Holforty, K. Kannan, V. Stepanyan and T. Lombaerts, "Adaptive Sensor Registration Across Distributed Airspace Surveillance Networks," in *AIAA SciTech*, Orlando , 2024.

[11] C. Ippolito, E. Kawamura, G. Gorospe, W. Holforty, K. Kannan, V. Stepanyan, T. Lombaerts, N. Brown, A. Jaffe and C. Dolph, "A Structurally-Adaptive Framework for Distributed Airborne Sensing over Real-time Collaborative Information Sharing Networks," in *AIAA SciTech*, Washington DC, 2023.

[12] C. Ippolito, K. Hashemi, E. Kawamura, G. Gorospe, W. Holforty, K. Kannan, V. Stepanyan, T. Lombaerts, N. Brown, A. Jaffe and C. Dolph, "Concepts for Distributed Sensing and Collaborative Airspace Autonomy in Advanced Urban Air Mobility," in *AIAA SciTech*, National Harbor, 2023.

[13] T. Lombaerts, K. Kannan, E. Kawamura, C. Dolph, V. Stepanyan, G. Gorospe and C. Ippolito, "Distributed Ground Sensor Fusion Based Object Tracking for Autonomous Advanced Air Mobility Operations," in *AIAA SciTech*, Washington DC, 2023.

[14] C. Dolph, C. Minwalla, L. Glaab, M. Logan, B. Allen and K. Iftekharuddin, "Detection and Tracking of Aircraft from Small Unmanned Aerial Systems," *Journal of Aerospace Information Systems,* vol. 18, no. 11, pp. 838-851, 2021.

[15] C. Dolph, C. Ippolito, L. Glaab, M. Logan, L. Tran, B. Allen, M. Alam, J. Li and K. Iftekharuddin, "Adversarial Learning Improves Vision-Based Perception from Drones with Imbalanced Datasets," *JOURNAL OF AEROSPACE INFORMATION SYSTEMS,* vol. 20, no. 8, pp. 489-507, 2023.

[16] F. Vitiello, F. Causa, R. Opromolla, G. Fasano, C. Dolph, T. Lombaerts and C. Ippolito, "Assessing Performance of Radar/Visual Fusion Techniques for Ground-to-Air Surveillance in Advanced Air Mobility: an Experimental Approach," in *IEEE/AIAA Digital Avionic Systems Conference*, Barcelona, Spain, 2023.

[17] F. Vitiello, F. Causa, R. Opromolla and G. Fasano, "Detection and tracking of non-cooperative flying obstacles using low SWaP radar and optical sensors: an experimental analysis," in *International Conference on Unmanned Aircraft Systems*, Dubrovnik, 2022.

[18] E. Kawamura, K. Kannan, T. Lombaerts, V. Stepanyan, C. Dolph and C. Ippolito, "Ground-Based Vision Tracker for Advanced Air Mobility and Urban Air Mobility," in *AIAA SciTech*, Orlando, 2024.

[19] F. Vitiello, F. Causa, R. Opromolla, G. Fasano, C. Dolph, T. Ferrante, T. Lombaerts and C. Ippolito, "Experimental Testing of Data Fusion in a Distributed Ground-Based Sensing Network for Advanced Air Mobility," in *AIAA SciTech Forum*, Orlando, 2024.

[20] V. Stepanyan, T. Lombaerts, C. Dolph, N. Cramer and C. Ippolito, "Estimation With Range Depended Sensor Model," in *AIAA SciTech*, SciTech, 2022.

[21] V. Stepanyan, K. Kannan, E. Kawamura, T. Lombaerts and C. Ippolito, "Distributed Target Tracking With Optimal Data Migration," in *AIAA SciTech Forum and Exposition*, National Harbor, MD, 2023.

[22] V. Stepanyan, C. Ippolito, K. Kannan, E. Kawamura, T. Lombaerts, W. Holforty and C. Dolph, "Flight Test Design and Implementation for Independent Surveillance of an Airspace Through a Distributed Ground Sensing Network," in *AIAA SciTech*, Orlando, 2024.

[23] S. Seidaliyeva, D. Akhmetov, L. Ilipbayeva and E. Matson, "Real-Time and Accurate Drone Detection in a Video with a Static Background," *Sensors,* vol. 20, no. 14, pp. 2-19, 2020.

[24] W. Nie, Z. Han, Y. Li, W. He, L. Xi and X. Yang, "UAV Detection and Localization Based on Multi-Dimensional Signal Features," *IEEE Sensors,* vol. 22, no. 6, pp. 5150-5162, 2022.

[25] S. Jamil, R. M. Fawad, A. Ullah, S. Badnava, M. Forsat and S. Mirjavadi, "Malicious UAV Detection Using Integrated Audio and Visual Features for Public Safety Applications," *IEEE Sensors,* vol. 20, no. 14, p. 3923, 2020.

[26] M. Campbell, D. Clark and F. Melo, "An Algorithm for Large-Scale Multitarget Tracking and Parameter Estimation," *IEEE Transactions on Aerospace and Electronic Systems,* vol. 57, no. 4, pp. 2053-2066, 2021.

[27] X. Yan, T. Fu, H. Lin, F. Xuan, Y. Huang, Y. Cao, H. Hu and P. Liu, "UAV Detection and Tracking in Urban Environments Using Passive Sensors: A Survey," *Applied Sciences,* vol. 13, no. 20, p. 11320, 2023.

[28] M. Pawełczyk and M. Wojtyra, "Real World Object Detection Dataset for Quadcopter Unmanned Aerial Vehicle Detection," *IEEE Access,* vol. 8, pp. 174394-174409, 2020.

[29] O. S. C. V. Library, "The OpenCV Reference Manual," 2024. [Online]. Available: https://github.com/itseez/opencv.

[30] E. Rosten, R. Porter and T. Drummond, "Faster and better: A machine learning approach to corner detection," *IEEE transactions on pattern analysis and machine,* vol. 31, no. 1, pp. 105-119, 2008.

[31] M. Muja and D. G. Lowe, "Fast approximate nearest neighbors with automatic algorithm configuration (2009)," in *VISAPP International Conference on Computer Vision Theory and Applications*, Lisboa, 2009.

[32] B. Lucas and T. Kanade, "An iterative image registration technique with an application to stereo vision," in *International Joint Conference on Artificial Intelligence*, British Columbia, 1981.

[33] A. Nussberger, Aerial Object Tracking from an Airborne Platform, Zurich: ETH Zurich Research Collection, 2015.

[34] U. Seidaliyeva, D. Akhmetov, L. Ilipbayeva and E. T. Matson, Real-Time and Accurate Drone Detection in a Video with a Static Background, vol. 20, Sensors, 2020.

[35] F. Fasano, D. Accardo, A. Tirri, A. Moccia and E. De Lellis, "Sky Region Obstacle Detection and Tracking for Vision-Based UAS Sense and Avoid," *Journal of Intelligent & Robotic Systems ,* vol. 84, pp. 121-144, 2016.

[36] R. Opromolla and G. Fasano, "Visual-based obstacle detection and tracking, and conflict detection for small UAS sense and avoid," *Aerospace Science and Technology,* vol. 119, no. 107167, pp. 1-20, 2021.

[37] M. Ester, H.-P. Kriegel, J. Sander and X. Xiaowei, "A density-based algorithm for discovering clusters in large spatial databases with noise," in *Proceedings of the Second International Conference on Knowledge Discovery in Databases and Data Mining*, Portland, 1996.

[38] J.-Y. Bouguet, "Camera Calibration Toolbox for Matlab," 14 Oct 2015. [Online]. Available: http://www.vision.caltech.edu/bouguetj/calib_doc/.

[39] M. Shuster and S. Oh, "Three-Axis Attitude Determination from Vector Observations," *Journal of Guidance and Control,* vol. 4, no. 1, pp. 71-77, 1981.

[40] T. Lombaerts, K. Shish, G. Keller, V. Stepanyan, N. Cramer and C. Ippolito, " Adaptive Multi-Sensor Fusion Based Object Tracking for Autonomous Urban Air Mobility Operations," in *AIAA SciTech* , San Diego , 2022.

[41] D. Locascio, M. Levy, K. Ravikumar, S. Briceno, B. German and D. Mavris, "Evaluation of Concepts of Operations for On-Demand Package Delivery by Small Unmanned Aerial Systems," in *AIAA AVIATION Forum*, Washington DC, 2016.

[42] E. Hunt and S. Rondon, "Detection of potato beetle damage using remote sensing from small unmanned aircraft systems," *Journal of Applied Remote Sensing,* vol. 11, no. 2, pp. 026013-026013, 2017.

[43] S. Dorafshan, R. Thomas, C. Coopmans and M. M., "Deep Learning Neural Networks for sUAS-Assisted Structural Inspections: Feasibility and Application," in *International Conference on Unmanned Aircraft Systems* , Dallas, 2018.

[44] K. Pratt, R. Murphy, S. Stover and C. Griffin, "CCONOPS and autonomy recommendations for VTOL small unmanned aerial system based on Hurricane Katrina operations," *Journal of Field Robotics,* vol. 26, no. 8, pp. 636-650, 2009.

[45] S. Ramasamy and R. Sabatini, "A Unified Approach to Cooperative and Non-Cooperative Sense-and-Avoid," in *International Conference on Unmanned Aircraft Systems (ICUAS)*, Denver, 2015.

[46] W. Kong, D. Zhang, X. Wang, X. Z. and J. and Zhang, "November. Autonomous landing of an UAV with a ground-based actuated infrared stereo vision system," in *International conference on intelligent robots and systems*, 2013.

[47] D. Comaniciu and P. Meer, "Mean shift: A robust approach toward feature space analysis," *IEEE Transactions on pattern analysis and machine intelligence,* vol. 24, no. 5, pp. 603-619., 2002.

[48] E. Johnson, A. Calise, Y. Watanabe, J. Ha and J. Neidhoefer, "Real-time vision-based relative aircraft navigation," *Journal of Aerospace Computing, Information, and Communication,* vol. 4, no. 4, pp. 707-738, 2007.

[49] C. Li, C. Xu, C. Gui and M. Fox, "Distance regularized level set evolution and its application to image segmentation," *IEEE Transactions on Image Processing,* vol. 19, no. 12, p. 3243–3254, 2010.

[50] R. Malladi, J. Sethian and B. Vemuri, "Shape modeling with front propagation: a level set approach," *IEEE Transactions: Pattern Analysis and Machine Intelligence,* vol. 17, no. 2, pp. 158–175,, 1995.

[51] E. Kawamura, C. Dolph, K. Kannan, N. Brown, T. Lombaerts and C. Ippolito, "VSLAM and Vision-based Approach and Landing for Advanced Air Mobility," in *AIAA SciTech*, Washington DC, 2023.

[52] E. Kawamura, C. Dolph, K. Kannan, T. Lombaerts and C. Ippolito, "Simulated Vision-based Approach and Landing System for Advanced Air Mobility," in *AIAA SciTech*, Washington DC, 2023.

[53] E. Kawamura, C. Dolph, K. Kannan, T. Lombaerts and C. Ippolito, "VSLAM and Coplanar POSIT for Advanced Air Mobility Approach and Landing," in *AIAA SciTech 2023* , National Harbor, MD, 2023.

[54] G. Fasano, D. Accardo, A. Tirri, A. Moccia and E. De Lellis, "Radar/electro-optical data fusion for non-cooperative UAS sense and avoid," *Aerospace Science and Technology,* vol. 46, pp. 436-450, 2015.